Fabrication and Application of 1653.7 nm Methane Sensor

Qingyun Xian, Hui Lv, Yucheng Yao, Chunfu Cheng, and Zhiqiang Zhou

***Abstract*—In industries such as coal mining, natural gas transportation and waste-to-energy, methane detection is an essential step. In order to reduce the risk and improve accuracy, laser sensors are used to detect methane. Aiming at the characteristics of the absorption peak of methane gas at 1653.7 nm, the 1653.7 nm distributed feedback laser was obtained from the multi quantum well materials design and ridge-wide pattern design to device packaging by using metal-organic chemical vapor epitaxial deposition, holographic exposure, and nanoimprint lithography. The laser performance achieves a side-mode suppression ratio of 54 dB, a slope efficiency of 0.372 W/A, a threshold current not greater than 12 mA, a saturated optical power greater than 20 mW, and stable optical and electrical properties. Based on this laser, for methane gas with a concentration of 0% to 3%, the loss is stable with the change of gas concentration, and the absorption sensitivity to methane is 0.20237 dB/%.**

***Index Terms*—Distributed feedback laser, 1653.7 nm laser, methane detection, frequency shift interferometric fiber cavity ring-down technology.**

I. Introduction

As ONE of the gases that cause the greenhouse effect, methane has a global warming potential of approximately 21 times that of carbon dioxide. Monitoring of methane is very important to reduce greenhouse gas emissions [1]. In addition, methane is flammable, explosive, and toxic. The frequent occurrence of explosions caused by methane leakage poses a threat to people's lives and property safety [2]. Therefore, it is very necessary to find a way to accurately monitor methane gas.

In daily life and industrial production, some harmful gases need to be constantly monitored for leakage or concentration measurement. In order to reduce the danger and pollution of measurement, there are mainly the following methods for gas detection: catalytic gas detection, electrochemical detection, infrared gas detection and tunable semiconductor laser detection [3]. Tunable semiconductor laser absorption spectroscopy (TDLAS) usually scans an independent gas absorption line with a single narrowband laser frequency. It features high selectivity and high resolution spectroscopy technology [4]. Due to the fingerprint characteristics of molecular spectrum, it is not interfered by other gases [5], [6]. Eric J. Zhang et al. developed a multi-section hybrid III-V silicon external-cavity laser, it demonstrates > 2 nm tunability and single-mode operation with SMSR > 50 dB for high-resolution spectroscopy [7]. The external cavity structure of the laser has the disadvantages of unstable structure and difficult mass production. The laser designed by us uses only a simple ridge waveguide structure, which is easy to process and has good reliability.

Compared with electrochemical and catalytic detectors, electrochemical and catalytic detectors are always in direct contact with gas, because the measurement principle is based on the chemical reaction that consumes the sensor material, they are prone to aging, and they are also sensitive to pressure and humidity changes. The laser gas sensor is an optical detector and has no direct contact with the gas, so it is not affected by poisoning or degradation at all. The humidity and pressure changes in the range of normal atmospheric conditions are not affected. Compared with infrared sensors, infrared sensors use infrared light as detection light. Water molecules have strong absorption characteristics in the infrared region, so infrared sensors have poor moisture resistance; The light source signal of infrared sensor is weak, usually it is necessary to distinguish between the standard gas chamber and the detection gas chamber to find the effective signal. Therefore, the air chamber will have a complex structure, weak anti-vibration ability, and is not suitable for mining areas. And the light source of the infrared sensor is very similar to the light source of the bulb, and it will become weaker over time, which affects stability. The laser sensor does not respond to steam, and its anti-vibration ability is also very good. The laser sensor module uses the most modern and stable semiconductor photoelectric components with a long service life.

One of the key technologies for trace detection of methane gas by absorption method is DFB laser diode (LD). Its performance characteristics require a single-mode laser with high signal-to-noise ratio, stable output, higher optical output power, lower temperature and current tuning rate, fast wavelength tuning, and stable spatial output characteristics [8].

Manuscript received 27 August 2022; accepted 2 September 2022. Date of publication 6 September 2022; date of current version 22 September 2022. This work was supporting in part by Enterprise Technological Innovation and Development Project in Hubei Province under Grant 2021BAB102 and in part by the Project of Outstanding Young and Middle-Aged Science and Technology Innovation Team of Colleges and Universities in Hubei Province under Grant T201907. *(Corresponding author: Hui Lv.)*

Qingyun Xian, Hui Lv, Yucheng Yao, and Chunfu Cheng are with the School of Chip Industry, Hubei University of Technology, Wuhan 430068, China (e-mail: xianqingyun@hbut.edu.cn; lvhui@hbut.edu.cn; yaoyucheng@hubt.edu.cn; chengchunfu@hbut.edu.cn).

Zhiqiang Zhou is with the Wuhan Mindsemi Company Limited, Wuhan 430079, China (e-mail: zhouzhiqiang@mindsemi.com).

Digital Object Identifier 10.1109/JPHOT.2022.3204674

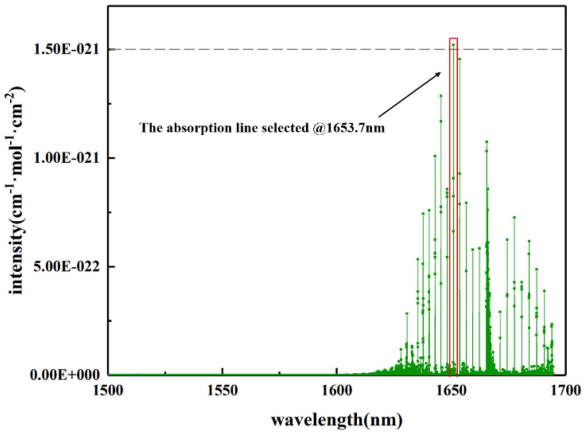

Fig. 1. Absorption line of CH_4 molecule.

II. Experiment

At 25 °C and standard atmospheric pressure, according to the HITRAN database, the absorption spectrum of CH_4 molecules in the range of 1500∼1700 nm is shown in Fig. 1. It can be clearly seen that at 1653.7 nm, the CH_4 molecule has the strongest absorption line, on the order of 10^{-21}. According to the principle of spectral absorption method, this peak value can be used as a basis for judging the existence of CH_4 gas.

The designed laser adopts a distributed feedback (DFB) structure. From bottom to top, the lower cladding layer, the multiple quantum well layer, the etching stop layer, the grating layer, the upper cladding layer, and the ohmic contact layer are sequentially grown on the InP substrate. The size of a single chip is 250∗250 μm. In practical application, there are many factors that cause the unstable working wavelength of laser. Therefore, the device must be temperature controlled, and the multi-quantum well adopts aluminium-free III-V materials. The active region is composed of 5 pairs of InGaAsP quantum wells and quantum barriers, of which the well is 5nm and the barrier is 9nm. In order to obtain a lower threshold current, the designed compressive strain is 1.2%. Holographic exposure method and nanoimprint lithography (NIL) are used to fabricate the DFB grating. The grating thickness of 15nm and the grating period of 254.9nm. Holographic method can flexibly adjust and optimize the grating period, and NIL has the advantages of large and uniform grating area. Therefore, the holographic exposure method was used to make the grating in the development of the sample, and then the parameters determined by the holographic method were transferred to NIL, and the high repeatability of the device performance and the high product yield were obtained. The peak wavelength of photoluminescence (PL) spectrum is around 1649nm. The epitaxial structure can obtain higher gain and lower threshold current at 1653.7 nm.

The chip production process mainly includes five photolithography:

The purpose of the first photolithography is to make the ridge. We first deposit a layer of SiN_x on the surface of the wafer. The appearance of the wafer is shown in Fig. 2. After the resist is applied, the designed mask is used for exposure and development. There is resist and SiN_x on the ridge. Then we etch the SiN_x to form shallow grooves on both sides of the ridge, remove the resist after etching, and the ridge is still protected by the SiN_x, and then perform InP etching. Then the SiN_x on the ridge is re-moved to form a trench with a depth of about 1.8 μm. The shape of the ridge is shown in Fig. 3.

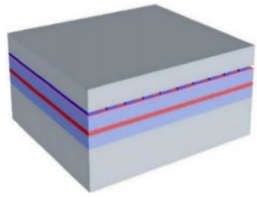

Fig. 2. The original structure.

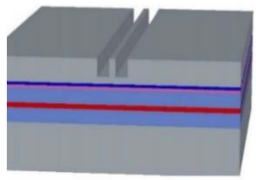

Fig. 3. The structure with ridge.

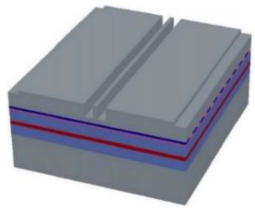

Fig. 4. The structure with cleavage.

The purpose of the second lithography is to make a cleavage area. We first deposit a layer of SiO_2, and then use the designed mask for exposure and development. There is only cleavage area without resist. After SiO_2 is etched and the resist is removed, the cleavage area is completed. The completed model of the cleavage area is shown in Fig. 4.

The purpose of the third photolithography is to protect the ridge sidewall SiO_2 from exposing the upper part of the ridge to facilitate gold plating. We first apply double layer resist and then use the designed mask to expose and develop, and then carry out resist etching. Since the resist in the groove is thicker than that on the ridge, there is still resist in the groove to protect the SiO_2 after the resist is etched. Then we perform SiO_2 etching to expose the upper part of the ridge and remove the resist.

The purpose of the fourth lithography is to make electrodes. We use the designed mask to expose and develop after the resist is applied, in order to expose the electrode part, and then evaporate the electrode part to plate gold, and then remove the resist and the electrode is completed as shown in Fig. 5.

The purpose of the fifth lithography is to thicken the electrode to increase heat dissipation. After the resist is applied, the designed mask is used for exposure and development, and then

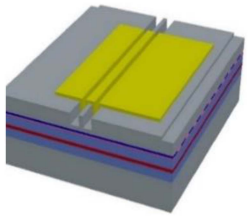

Fig. 5. The structure with electrodes.

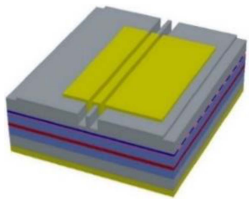

Fig. 6. The final structure.

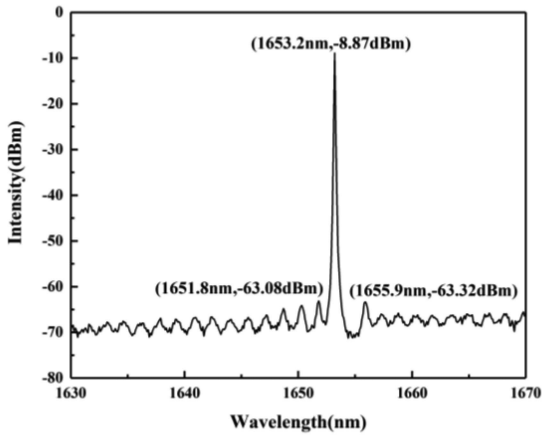

Fig. 7. chip wavelength test.

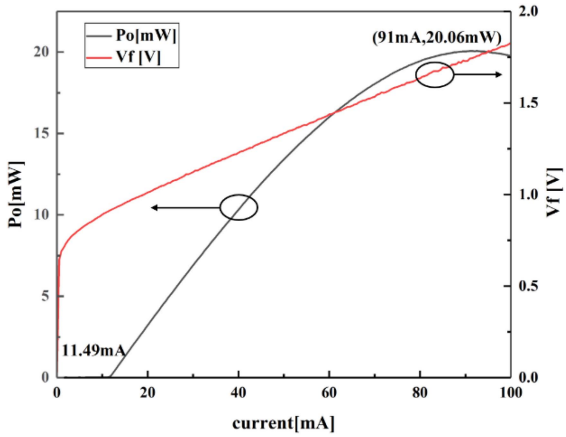

Fig. 8. Chip optical power output and voltage changes with current.

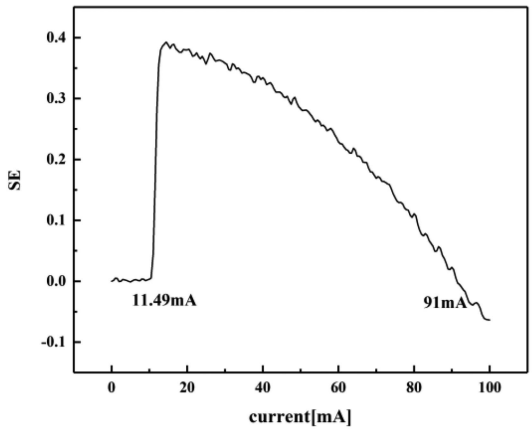

Fig. 9. Chip slope efficiency.

electroless gold plating is performed to increase the gold on the electrode surface to the target thickness. Then the wafer is thinned and polished, and the back electrode is made as shown in Fig. 6. After the production is completed, we first disassemble the wafer into strips, and coat the end faces on both sides with anti-reflection coating and high-reflection coating to improve the single-mode performance and side mode suppression ratio.

III. Results and Discussions

The chip performance test mainly screens the chip's threshold current, optical output power, slope efficiency, peak wavelength, and SMSR. The peak wavelength is the lasing wavelength. As shown in Fig. 7, at 25 °C, the chip peak wavelength is 1653.2 nm and the intensity is −8.87 dBm. The SMSR is the ratio of the optical intensity of the main mode to the most significant side mode. The most prominent side mode is the peak at 1651.8 nm, the intensity is −63.08 dBm, and the SMSR is 54.21; the threshold current is the minimum current that the chip can lasing. Fig. 8 shows that the threshold current is 11.49 mA. As the current increases, the optical output power reaches saturation at 91mA, and the saturated optical power is 20.06 mW. Fig. 9 shows the slope efficiency of the chip, which reflects the rate of increase of the optical output power. It is 0.383 W/A at the maximum under the threshold current. It gradually decreases as the current increases, and becomes a negative value when it reaches saturation.

The chip package TO-56 (Transistor Outline) is subjected to reliability testing and electrostatic testing. Reliability testing is divided into two stages: burn-in and aging. The first stage uses a high temperature of 100 °C and a high current of 80 mA for 48 hours. The purpose of this stage is to eliminate early failure products. In the second stage, a long-term life test is carried out at a temperature of 85 °C and a current of 80 mA. The Fig. 10 below shows the result of the life test of the chip for 1600 hours. It can be found that the backlight intensity is relatively small under high temperature and high current for 48 hours in the first stage, but no failure occurs, and the backlight intensity is stable under appropriate conditions in the second stage. The overall fluctuation of the backlight intensity is caused by the opening and closing of the aging box. Except for the overall fluctuation, the backlight intensity of each chip does not fluctuate greatly,

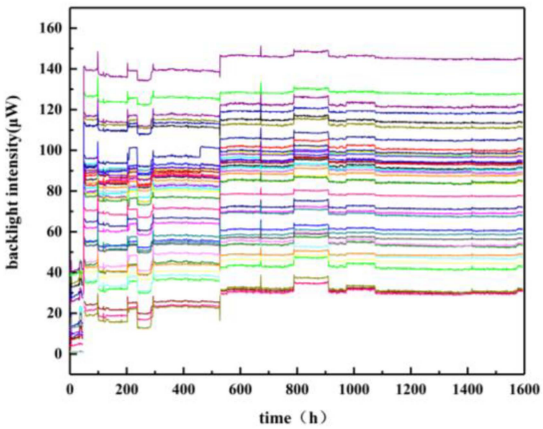

Fig. 10. 1600 hours reliability test results.

Fig. 11. TO-56 package appearance.

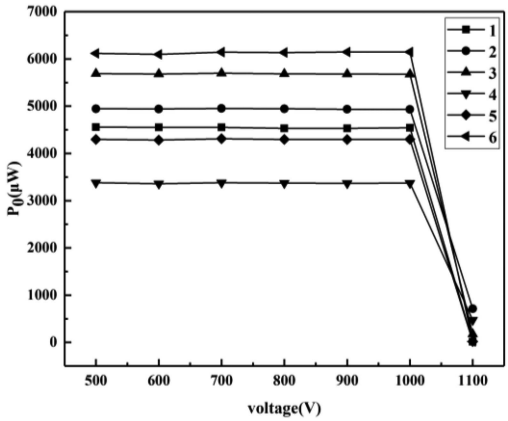

Fig. 12. ESD test results.

and the reliability is good. The appearance of the TO-56 package is shown in Fig. 11.

The electro-static discharge (ESD) is used to test the chip's ability to withstand static electricity. The following Fig. 12 shows the test result of the chip starting from 500 V to 1100 V in 100 V increments. The result shows that the maximum static voltage that the chip can withstand is about 1000 V, which meets the needs in practical applications.

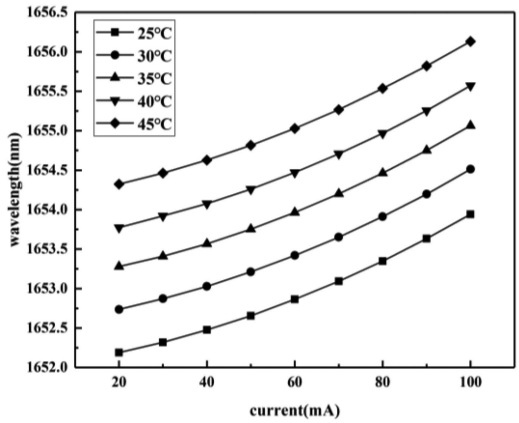

Fig. 13. Variation of COC lasing peak wavelength with current at different temperatures.

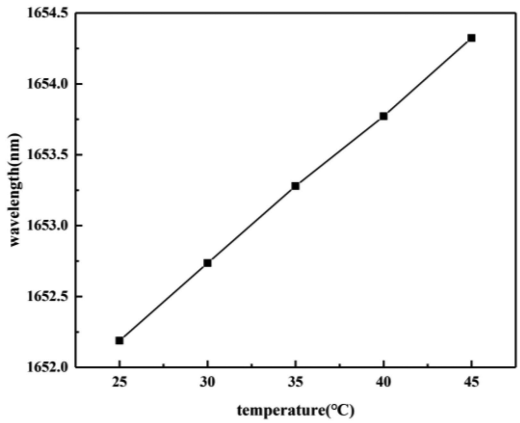

Fig. 14. COC lasing peak wavelength changes with temperature at 50 mA.

The purpose of making the chip COC (chip on carrier) is to test the wavelength change with temperature and current, and to check whether the wavelength exceeds the tuning range due to temperature and current changes in actual use, causing monitoring errors. COC is to solder the chip on the transition block, connect the chip electrode and the transition block with gold wires, place it on the TEC (Thermoelectric Cooler) to control the test temperature, and use metal probes to add different currents. Fig. 13 shows the variation of COC lasing peak wavelength with current at different temperatures, the slope of each curve is the drift coefficient of wavelength with current; Fig. 14 shows the drift coefficient of the test peak wavelength with temperature under 50 mA, changing the temperature from 25 °C to 45 °C, that is, the change rule of the five curves in Fig. 14 at 50 mA. By fitting the test data, the drift coefficients of wavelength with temperature and current can be derived as: $\Delta\lambda/\Delta I \approx 0.022$ nm/mA; $\Delta\lambda/\Delta T \approx 0.107$ nm/ °C.

IV. Methane Gas Detection

The methane detection experiment is based on the frequency-shift interference fiber cavity ring-down technology proposed

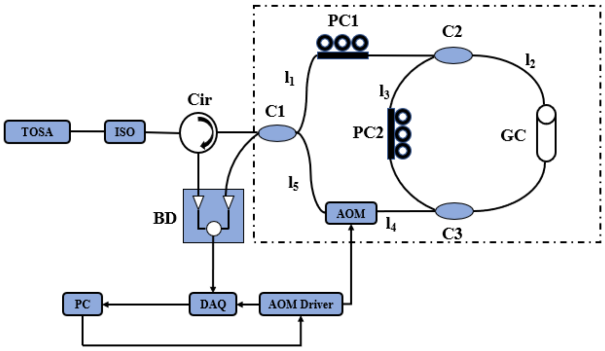

Fig. 15. Block diagram of frequency-shifted interferometric cavity ring-down sensing system.

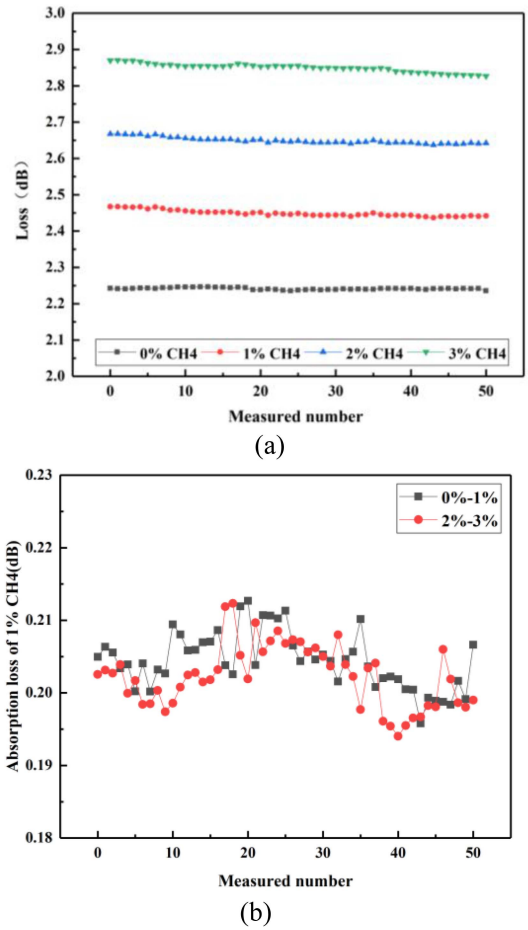

Fig. 16. (a) Absorbtion loss of gas chamber filled with different concentrations of methane (b) Absorption loss of 1% concentration of methane.

by Cheng Chunfu et al [9]. The fabricated chip is packaged into transmitter optical subassembly (TOSA) as a laser light source for methane detection experiment. The experimental system diagram is shown in Fig. 15 below. The system includes a fiber cavity ring-down frequency-shift interferometer, a laser light source (TOSA), a fiber circulator, an acousto-optic modulator (AOM) and its drive, a balanced detector (BD), and a data acquisition card (DAQ) and computer (PC). Among them, the fiber

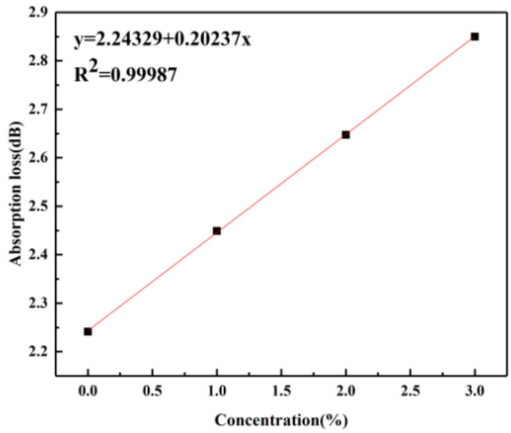

Fig. 17. Absorption loss corresponding to different concentrations of methane and its fitting.

cavity ring-down frequency-shift interferometer is con-structed by inserting a frequency shifter (AOM) asymmetrically in the ring, and inserting a fiber ring-down ring, as shown by the dashed box in Fig. 16. Among them, C1 is a 50/50 fiber coupler; C2 and C3 are 99.5/0.5 fiber couplers; GC is a micro gas cell. PC1 and PC2 are polarization controllers. A coupler with a high split ratio is used in the ring-down ring. Most of the light entering the ring-down ring continues to transmit in the ring, and a small part is absorbed by the gas chamber, which increases the number of turns of light transmission in the ring and makes the experimental results easier measurement.

As shown in Fig. 16(a), we tested the empty cavity (filled with pure nitrogen), the cavity loss of 1%, 2% and 3% methane concentration, each concentration measured 50 samples, it can be found that as the methane concentration in the gas chamber in-creases the cavity loss will also become larger. As shown in Fig. 16(b), by comparing the loss from 0% to 1% and from 2% to 3%, the absorption loss of 1% methane fluctuates in the range of $\pm$0.0095 dB, indicating that the system has a good stability. As shown in Fig. 17, fitting the average value of the gas cell loss at the three concentrations yields a methane absorption sensitivity of 0.20237 dB/%. Experiments show that the laser can meet the needs of actual methane detection.

V. Conclusion

A DFB chip with low threshold and high power, high side-mode suppression ratio and mode stability matching the absorption peak of methane gas at 1653.7 nm was developed. The methane detection experiment using the frequency-shifted interference fiber cavity ring-down technology proves that the frequency-shifted interference fiber cavity ring-down system based on the light source has stable loss with the change of gas concentration, and the absorption sensitivity to methane is 0.20237dB/%. The pro-duction process is simple, the yield is high, and the devices can be produced in batches. Reliability experiments show that the device has long-term stability and can meet the needs of practical applications such as monitoring natural gas leakage in kitchens and gas detection in coal mines.

REFERENCES

[1] M. Xue et al., "Current status on fugitive methane emission measurements and inventory during oil and gas production," *Adv. Climate Change Res.*, vol. 15, no. 2, pp. 187–195, 2019, doi: 10.12006/j.issn.1673-1719.2018.118.

[2] J. Kamieniak, E. P. Randviir, and C. E. Banks, "The latest developments in the analytical sensing of methane," *TrAC Trends Anal. Chem.*, vol. 73, pp. 146–157, Nov. 2015, doi: 10.1016/j.trac.2015.04.030.

[3] Y. Liu et al., "The simulation research of gas absorption process based on TDLAS," *Laser J.*, vol. 38, no. 3, pp. 37–40, 2017, doi: 10.14016/j.cnki.jgzz.2017.03.037.

[4] C. Li et al., "Compact mid-infrared trace gas detection system based on TDLAS and ICL," *Opt. Precis. Eng.*, vol. 26, no. 8, pp. 1855–1861, Aug. 2018, doi: 10.3788/OPE.20182608.1855.

[5] O. Aiguo et al., "Detection of key performance indicators of ethanol diesel by the infrared spectroscopy method," *Chin. Opt.*, vol. 10, no. 3, pp. 363–369, Jun. 2017, doi: 10.3788/co.20171003.0363.

[6] W. Nie et al., "Measurement of low water vapor dew-point temperature based on tunable diode laser absorption spectroscopy," *Opt. Precis. Eng.*, vol. 26, no. 8, pp. 1862–1869, Aug. 2018, doi: 10.3788/OPE.20182608.1862.

[7] E. J. Zhang et al., "Methane absorption spectroscopy with a hybrid III-V silicon external cavity laser," in *Proc. Conf. Lasers Electro-Opt.*, May 2018, pp. 1–2, doi: 10.1364/CLEO_SI.2018.STh1B.2.

[8] S. Wang et al., "Research on fiber-optic sensors for methane detection based on Harmonic detection," *Proc. SPIE Int. Soc. Opt. Eng.*, vol. 7656, pp. 707–712, 2010, doi: 10.1117/12.871963.

[9] C. Cheng et al., "Simultaneous measurement of gas composition and concentration combined fiber cavtiy ringdown and frequency-shifted interferometry," *Opt. Fiber Technol.*, vol. 48, pp. 303–307, 2019, doi: 10.1016/j.yofte.2019.01.032.